

Driven power-law oscillator

Peter Schmelcher*

Zentrum für Optische Quantentechnologien, Universität Hamburg, Luruper Chaussee 149, 22761 Hamburg, Germany and Hamburg Centre for Ultrafast Imaging, Universität Hamburg, Luruper Chaussee 149, 22761 Hamburg, Germany

(Received 3 June 2018; revised manuscript received 23 July 2018; published 24 August 2018)

We explore the nonlinear dynamics of a driven power-law oscillator whose shape varies periodically in time covering a broad spectrum of anharmonicities. Combining weak and strong confinement of different geometry within a single driving period, the phase space allows not only for regular and chaotic bounded motion but in particular also for an unbounded motion which exhibits an exponential net growth of the corresponding energies. Our computational study shows that phases of motion with energy gain and loss as well as approximate energy conservation alternate within a single period of the oscillator and can be assigned to the change of the underlying confinement geometry. We demonstrate how the crossover from a single- to a two-component phase space takes place with varying frequency and amplitude and analyze the corresponding volumes in phase space. In the high-frequency regime an effective potential is derived that combines the different features of the driven power-law oscillator. Possible experimental realizations are discussed.

DOI: [10.1103/PhysRevE.98.022222](https://doi.org/10.1103/PhysRevE.98.022222)

I. INTRODUCTION

Many physical systems can be modeled and described to some approximation by individual oscillators or a collection of interacting oscillators. Examples are vibrating molecules, phonons in solids, and coupled Josephson junctions. The route to complexity in the sense of a many-faceted dynamical behavior is then at least twofold: either one increases the number of (interacting) oscillators at the cost of dealing with a high-dimensional generally mixed regular-chaotic phase space, or one stays in low spatial dimensions and accounts for a nonintegrable modification of the underlying integrable oscillator. The latter case not only has been a paradigm for the route to chaos in low-dimensional systems but also showcases many mechanisms of universal character that are valid also for higher-dimensional setups. In the present work we will pursue this second route and introduce a type of one-dimensional driven oscillator that unites properties usually occurring for different dynamical systems. Before doing so and in order to provide a proper embedding and bottom-up approach in terms of complexity, let us briefly touch upon some important basic facts concerning oscillators and dynamical billiards in low dimensions.

For the one-dimensional harmonic oscillator exposed to dissipation and forcing closed form analytical expressions are available [1] for arbitrary time-dependent external forces. In case of a periodic driving and for vanishing dissipation the motion is nonresonant, regular and bounded if the frequency of the driving is unequal the one of the harmonic confinement. It is only for the resonant case of equal frequencies that a linearly in time diverging amplitude is encountered. Nonlinear oscillators such as the Duffing oscillator [2,3] or the kicked rotor (see Refs. [4,5] and references therein) represent

prototype systems whose phase space decomposition varies from regular to mixed and finally predominantly chaotic with correspondingly changing parameters. Specifically the kicked rotor exhibits a transition from a motion with bounded energy to a diffusive dynamics. The latter leads to an unbounded momentum increase, and a linear increase of the energy in time takes place beyond a critical kicking strength. Switching from an external driving force to a parametric driving the harmonic oscillator can gain energy for certain frequency ratios of the natural frequency compared to the parametric driving frequency. The maximum gain and exponential growth of the oscillation amplitude occurs for a ratio of one half, and the oscillator then phase locks to the parametric variation [6].

On the other hand, Fermi acceleration (FA) [7], which refers to the unbounded growth of the energy of particles while repeatedly colliding with moving massive objects or fields, has been of interest over many decades. Prototype models showing FA are time-dependent hard wall two-dimensional billiards which have come into the particular focus of exponential FA during the past 10 years [8–14]. Under certain conditions exponential FA can take place for most initial conditions. This has been demonstrated for the rectangular billiard with an oscillating bar [9–11] and for a class of chaotic billiards that exhibit a separation of ergodic components [12,13]. Importantly, it has been shown recently [14,15] that under very general conditions a generic time-dependent two-dimensional billiard exhibits FA in the adiabatic limit. A key ingredient therefore is that the corresponding static, i.e., time-independent, counterpart of the billiard exhibits a mixed regular-chaotic phase space. However, the situation is very much different in a single spatial dimension. Here the prototype billiard is the well-known Fermi-Ulam model describing a particle that multiply collides with moving walls [16]. The Fermi-Ulam model does not allow for FA at all, and in particular not for the exponential FA, if the applied time-dependent driving law is sufficiently smooth.

*Peter.Schmelcher@physnet.uni-hamburg.de

This is due to the existence of invariant tori which suppress the global energy transport [17].

The current work goes one step further in the above line and introduces the driven or time-dependent power-law oscillator (TPO). Opposite to the above-mentioned cases, where the (harmonic) confinement of the oscillator remains intact during the external forcing, this is not the case anymore for the TPO. Here the confinement itself becomes time-dependent, or, put it another way, the exponent of the power-law potential becomes time dependent. Specifically we focus on the case of a periodic driving characterized by a frequency and an amplitude as well as a constant offset. Within a single driving period phases of strong and weak anharmonic confinement follow upon each other thereby covering a continuous interval of power-law confinement strengths. Our aim is to provide a first computational study of this driven power-law oscillator with an emphasis on the analysis of its phase space. The latter is straightforwardly possible due to the low dimensionality of the TPO. As we shall see this peculiar oscillator provides an unusual combination of dynamical features which one might not suspect to appear from a first glance at its Hamiltonian and from the preexperience gained from the “traditional” oscillators. Obviously the TPO characterized by the time-dependent “pumping” of its anharmonicity is very much different from the billiard dynamics. Nevertheless the question for a comparison of their energy growth behavior is an intriguing one.

In detail we proceed as follows. In Sec. II we introduce our setup and in particular the underlying time-dependent model Hamiltonian for the TPO. We discuss the properties of the instantaneous one-dimensional potential whose confinement behavior changes qualitatively for different times. The underlying phase space is equally considered. Section III provides an analysis of the dynamics, first, by inspecting trajectories and, second, by investigating the Poincaré surfaces of section. This allows us to gain an overview of the dynamical components in phase space. A quantification of the volume of the different components of the phase space is provided. Subsequently the time evolution of the energy behavior for an ensemble is provided. This section contains also a discussion of the high-frequency regime. We present our conclusions and outlook in Sec. IV.

II. SETUP, HAMILTONIAN, AND STATIC PHASE SPACE

The TPO as defined below is motivated by the idea that a most general oscillator would also allow for a time-dependent variation of the geometry of the spatially confining potential. This is obviously not the case for the harmonic oscillator exposed to an external forcing, the Duffing oscillator, or the parametric oscillator with a time-dependent frequency. The most straightforward possibility to change the shape of the potential time dependently is to maintain its power-law appearance but make the exponent time dependent. The TPO Hamiltonian then reads

$$\mathcal{H} = \frac{p^2}{2} + \alpha q^{2\beta(t)} \quad (1)$$

and contains the time-dependent potential $V(q, t) = \alpha q^{2\beta(t)} := \alpha(q^2)^{\beta(t)}$. The latter is a defining equation which ensures a positive real argument and implies that the positive

real root always is taken for arbitrary powers β . For reasons of simplicity we set the mass of the oscillator to one. Our focus in this work is on a periodic time dependence of the exponent $\beta(t) = \beta_0 + \beta_1 \sin(\omega t)$, which contains the amplitude β_1 of the sinusoidal driving and the constant offset β_0 . $\alpha = 1$, $\beta_0 = 1$ will be chosen throughout, which means that the oscillation takes place around the harmonic oscillator potential αq^2 as an equilibrium configuration. Depending on the amplitude β_1 the TPO possesses alternating phases of strong and weak anharmonic confinement covering continuously the noninteger powers within an individual oscillation.

It should be noted that, due to the occurrence of arbitrary fractional powers already in the Hamiltonian (1), an analytical approach of whatever kind is in general not obvious. The reason therefore is that the resulting integrals cannot be evaluated analytically. For the numerical solution of the resulting equations of motion we employ a fourth-order Adams-Moulton predictor corrector integrator. However, one has to take into account the singularities of the potential and its derivatives. Indeed, $V(q, t)$ becomes singular at $q = 0$ for $\beta(t) < 0$ if $\beta_1 > \beta_0$. Equally the first and second derivative become singular at $q = 0$ for $\beta_1 > \beta_0 - \frac{1}{2}$ and $\beta_1 > \beta_0 - 1$, respectively. Therefore a regularization of the equations of motion is appropriate. We accomplish this by replacing the potential $V(q, t) = \alpha q^{2\beta(t)}$ by its regularized version $V(q, t) = \alpha(q^2 + C)^{\beta(t)}$. C is chosen to be a very small (typical value of the order of 10^{-8}) positive constant removing all singularities at the origin. The impact of this tiny regularization constant on the actual motion is very limited and controllable. For the case $\beta \gtrsim 1$ one can estimate the impact of $C \neq 0$ on the dynamics by calculating the relative change of the velocity in a corresponding “collision.” This amounts to $\frac{\Delta v}{v} = 2\alpha\beta \frac{C^\beta}{v^{2\beta}}$, which is for small C and a very large range of velocities a tiny correction. Moreover, for $\beta \ll 0.5$

one can show that the spatial extension $\Delta x = 2[(\frac{y}{\alpha})^{\frac{1}{\beta}} - C]^{\frac{1}{2}}$ on which the potential acquires values $y \ll 0.1$ decreases rapidly to zero, which also renders the impact of a correspondingly small $C \neq 0$ very small [see Fig. 1(a) for the cusp at the origin].

Since the TPO (1) is of quite an unusual appearance let us first discuss the instantaneous form of the potential as the time evolution proceeds. This evolution is illustrated in Fig. 1(a). For values $\beta > 1$ the nonlinear confinement is stronger (for $q > 1$) than that of the harmonic oscillator covering in time a continuous range of exponents $1 < \beta < 1 + \beta_1$ where the curvature is always positive.

For values $0.5 < \beta < 1$, however, the curvature decreases and for $\beta = 0.5$ $V(q)$ becomes linear. Further decreasing its value ($0 < \beta < 0.5$) the potential shows now a very weak confining behavior and exhibits a negative curvature. Here the formation of a negative cusp of $V(q)$ can be observed [note that $V(0) = 0$ for $C = 0$ holds also in this regime]. Due to this cusp the dynamics close to the origin of such a (static) potential experiences kicks, i.e., sudden changes of the underlying momentum. How much of the above qualitatively very different behavior of the instantaneous potential $V(q)$ is covered for a corresponding TPO (1) depends of course on the value of the amplitude β_1 .

The corresponding instantaneous phase space is illustrated in Fig. 1(b). For $\beta > 1$ the phase space curves are convex, but for $\beta < 1$ they develop a cusp at $q = 0$ and become

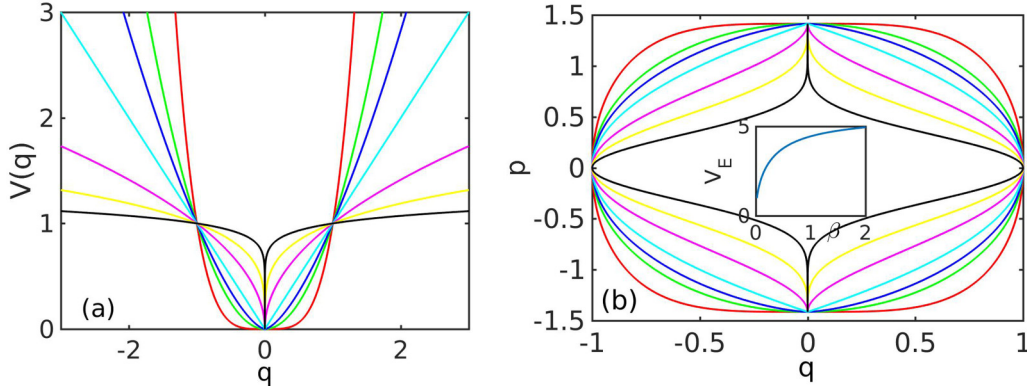


FIG. 1. (a) Snapshots of the potential $V(q)$ for different instantaneous values of the parameter β . Red, green, blue, cyan, magenta, yellow, and black lines correspond to the values $\beta = 2, 1, 0.75, 0.5, 0.25, 0.125, 0.05$ ordered according to their appearance from top to bottom for $q > 1$. (b) Phase space (q, p) curves for the same values of β following the identical color coding. The energy chosen is $E_0 = 1$. The central inset shows the volume V_E of the phase space for energies $E \leq E_0$ as a function of the parameter β (see text).

piecewise concave. The total phase space volume bounded by the energy shell with energy E_0 , i.e., the volume of the set $\{(q, p) | E(q, p) \leq E_0\}$ for a fixed E_0 , is given by $V_E = \int_{\mathcal{H}(q, p) \leq E_0} dp dq$. Note that this quantity represents in ergodic systems an adiabatic invariant [18]. V_E is shown in the central inset of Fig. 1(b), and we observe that it shrinks monotonically with decreasing β . In particular also the average width in momentum space decreases with decreasing β . Close to maximal momenta are then accessible only in the vertical channels around $q = 0$, which become increasingly narrow with decreasing β .

III. RESULTS AND DISCUSSION

Due to the three-dimensional (q, p, t) character of our system a complete overview of phase space can be achieved by performing stroboscopic snapshots in time for each period $T = \frac{2\pi}{\omega}$. One might expect that the intermediate-frequency regime (for which the driving frequency ω and the natural frequency of the time-independent oscillator are comparable) is the most interesting. Then a mixed phase space of regular and chaotic motion, depending on the size of the oscillation amplitude, could be expected. The high-frequency and low-frequency motion could be predominantly regular at least for small amplitude. A natural question to pose is: How does the energy transfer to the oscillator take place and what is the time evolution of its energy? Does the energy stay bounded or become unbounded, and if the latter occurs, is the increase of power-law or of exponential character? From the quasistatic picture discussed in Sec. II one might conjecture that during the half-period of each cycle of the driving for which $\beta > \beta_0$ the strong confinement prevents the oscillator from attaining a large amplitude and therefore energy and vice versa for the other half-cycle for which $\beta < \beta_0$.

A. A first glance at the dynamics: Trajectories

In order to gain a first insight into the dynamical behavior of the driven power-law oscillator it is instructive to consider individual trajectories. The decisive parameters to be varied

for fixed $\beta_0 = 1, \alpha = 1$ are the amplitude of the oscillation β_1 and the underlying frequency ω .

Let us briefly discuss some relevant aspect concerning the initial conditions (ICs) of the trajectories for given parameters of the oscillator. For the time-independent oscillator for arbitrary values of β the distance of the IC from the origin ($q = 0, p = 0$) in phase space plays no essential role for the resulting phase space curves. Their overall shape remains the same. However, as we shall see below, this distance is crucial for the individual trajectory dynamics of our TPO. Therefore, we shall choose in the following as examples ICs close to and far from the origin. The origin itself is a fixed point of the dynamics in all cases of the TPO, i.e., for arbitrary parameter values, while it might change its stability character (see below). The latter is not possible for the time-independent oscillator where this fixed point is always stable for $\beta > 0$.

Let us begin with the case $\beta_1 = 0.1, \omega = 0.1$ which is the case of comparatively small amplitude and low frequency. Figure 2(a) shows for the IC $[q(t=0) = 1, p(t=0) = 1]$, i.e., close to the origin, the time dependence of the energy. It exhibits two frequencies. The smaller one corresponds to the driving frequency ω and the larger one to the instantaneous oscillator frequency. The latter varies not significantly due to the small amplitude β_1 in this case. Note that the overall variation of the energy is very small and amounts to less than 1% of the initial energy $E(t=0)$. The inset in Fig. 2(a) shows the corresponding phase space curves, which, on the given timescale, shows small deviations from the time-independent case. In Fig. 2(b) for the same setup the IC $(-30, 20)$ is chosen, i.e., an IC far from the central fixed point. Here we observe a large variation of the energy with time of more than 50% of the initial energy. Still the energy shows bounded oscillations with essentially two frequencies. The smaller one again corresponds to the driving frequency ω and the larger one [note that the corresponding oscillation is hardly visible in Fig. 2(b) due to the small amplitude] to the instantaneous oscillator or confinement frequency. The corresponding phase space curves in the inset show now significant deviations from the initial winding of the phase space trajectory, thereby changing its overall anisotropic shape.

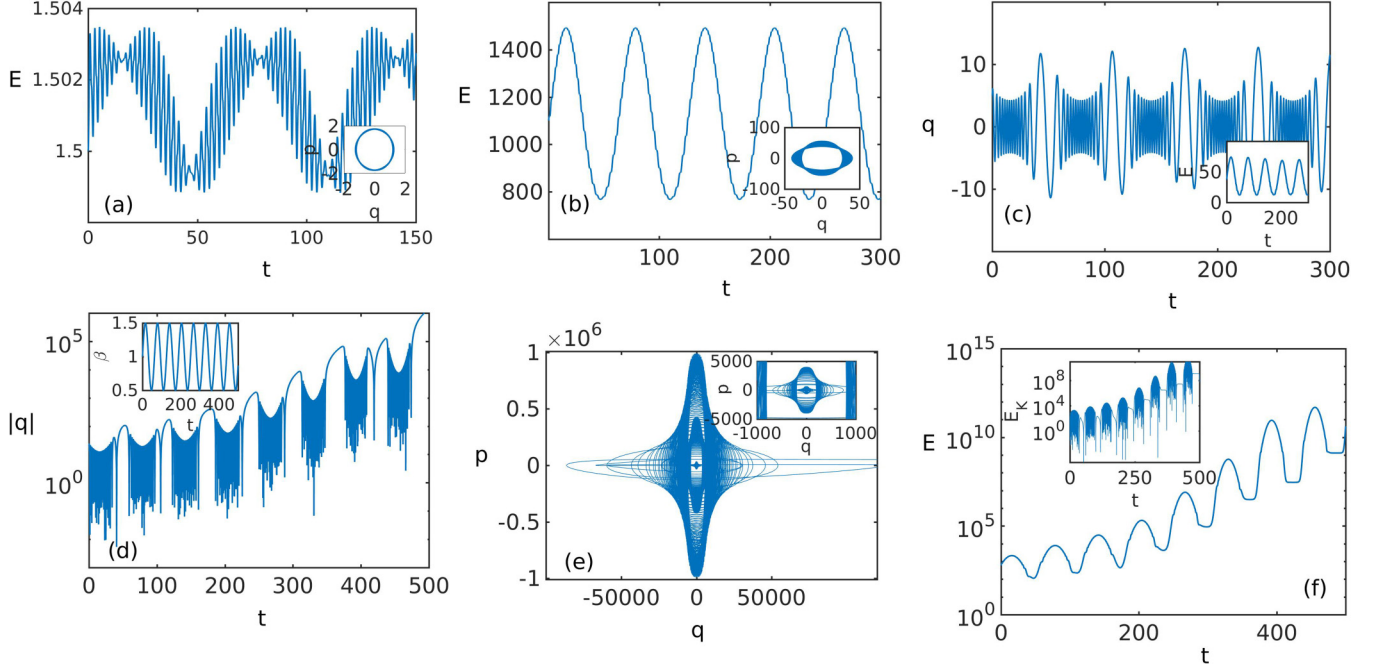


FIG. 2. Trajectories of the TPO for $\omega = 0.1$ with varying amplitude β_1 . (a) Total energy $E(t)$ as a function of time and in the inset the covered phase space $[q(t), p(t)]$ during the same time period for the IC $q(t=0) = 1$, $p(t=0) = 1$ for $\beta_1 = 0.1$. (b) Same as for (a) but for the IC $q(t=0) = -30$, $p(t=0) = 20$. (c) Amplitude $\beta_1 = 0.5$; the time evolution of the coordinate $q(t)$ and in the inset the corresponding total energy $E(t)$ for the IC $q(t=0) = 5$, $p(t=0) = 5$. (d) $\beta_1 = 0.5$: the time evolution of the absolute value $|q|(t)$ for the IC $q(t=0) = 20$, $p(t=0) = 20$ together with $\beta(t)$ in the inset. (e) Same parameter values as in (c, d), but showing the corresponding phase space curves $[q(t), p(t)]$ on different scales (zoom in for inset) and (f) showing the corresponding time evolution of the total (main figure) and kinetic energies (inset) for the same IC.

The dynamics changes qualitatively if we consider the situation of an increased amplitude. Figures 2(c)–2(f) analyze the dynamics again for a low-frequency $\omega = 0.1$ but a substantially increased amplitude $\beta_1 = 0.5$ such that the oscillator potential changes between $|q|$ and $|q|^3$ (assuming $C = 0$), which covers a broad interval of anharmonicities of fractional powers. Figure 2(c) shows the time evolution in coordinate space $q(t)$ for the IC (5,5). The envelope behavior obeys the frequency $\omega = 0.1$, but now a strong chirp of the frequency of the individual oscillations can be observed. Large-amplitude behavior occurs for low frequencies, whereas small amplitudes occur at high frequencies. The inset demonstrates that a large variation of the underlying energy $E(t)$ takes place at the frequency ω (the larger frequency and small-amplitude oscillations are hardly visible in the inset). We emphasize that all the dynamics observed so far is regular, i.e., periodic and quasiperiodic, and in particular bounded, which holds also for the corresponding energy.

The above situation changes if we consider an IC (20,20) farther away from the stable elliptic fixed point of the TPO at the origin. Figure 2(d) shows $|q|(t)$ on a semilogarithmic scale as a function of time for a somewhat longer time interval as compared to Fig. 2(c). Here we observe in the average an exponential increase of the amplitude of the coordinate oscillations, which equally cover positive and negative values. Periods of high-frequency and smaller-amplitude motion are intermittently interrupted by periods of lower-frequency large-amplitude motions. With the help of the corresponding inset showing $\beta(t)$ the latter can be assigned to the overall

periodic oscillations of the TPO. For time intervals where the power of the oscillator covers the interval $1 \leq 2\beta \leq 2$, i.e., if the oscillator confinement weakens from quadratic to linear, large-amplitude excursions occur. For time intervals with $2 \leq 2\beta \leq 3$, i.e., if the oscillator confinement increases up to a cubic behavior, the high-frequency small-amplitude oscillations are encountered. Figure 2(e) shows the corresponding phase space curves $[q(t), p(t)]$. Extending on the discussion of the anisotropically evolving phase space curves, according to the inset of Fig. 2(b), we now observe that this pattern repeats subsequently on different length scales. This is shown in Fig. 2(e) and its inset for a zoom into the central part of the phase space. According to the observed exponential scaling the winding of the phase space curves at high frequency on their individual length scales is connected by low-frequency intermediate transients which connect the different length scales. The dynamics therefore repeats as time proceeds on different length scales in a self-similar fashion, which can nicely be seen in Fig. 2(e). Finally Fig. 2(f) shows the time evolution of the corresponding total energy $E(t)$ and kinetic energy $E_K(t)$ in the inset on a semilogarithmic scale. During the time intervals of low-frequency high-amplitude motion of $|q|(t)$ [see Fig. 2(d)] a plateau-like behavior is observed for the energy $E(t)$. During the high-frequency small-amplitude motion of $|q|(t)$ a strong increase and decrease of the total energy can be observed. $E(t)$ increases strongly when the amplitude of the high-frequency oscillations decreases and vice versa. In the average the total energy increases exponentially. As a matter of precaution, we note that this

and similar statements are to be understood within our finite time simulations of a finite portion of the TPO phase space. A similar behavior can be observed for the kinetic energy E_K in the inset of Fig. 2(f) which demonstrates in particular that the kinetic energy also grows on the average exponentially. The kinetic energy becomes large during intervals of motion of the TPO with strong confinement $2 \leq \beta \leq 3$, i.e., when the TPO compresses and “pumps” the motion. Low kinetic energies occur for the intervals of motion $1 \leq \beta \leq 2$ of the TPO where it releases the motion to a much less confining potential. The latter interval coincides with the plateau-like behavior of the total energy, i.e., we have approximately no increase or decrease of the total energy.

Already the above-analyzed few trajectories for given parameter values exhibit a rich behavior of the TPO dynamics. Having this in mind, let us now gain an overview of complete phase space by inspecting the corresponding Poincaré surfaces of section (PSS). These PSS are stroboscopic snapshots of the dynamics at periods of the external driving. We will explore the PSS with varying parameters.

B. Poincaré surfaces of section

Our few above-analyzed example trajectories have been focusing on the low-frequency case. We have observed that with increasing amplitude β_1 of the TPO there exist not only regular trajectories with bounded energy oscillations, but also trajectories that exhibit an exponential increase in position and energy. In the following we discuss the corresponding PSS of our TPO for different frequencies ω and amplitudes β_1 . In this way we will gain a more complete overview of phase space with varying parameters. Note, that due to the fact that the phase space of the TPO is unbounded from above, the following computational studies focus on a finite but quite large energy window above zero energy. The minimal zero energy is given by the fixed point at the origin (assuming $C = 0$).

Figure 3(a) shows the PSS for a comparatively low-frequency $\omega = 0.1$ and small-amplitude $\beta_1 = 0.1$ corresponding to the trajectories shown in Figs. 2(a) and 2(b). All of the phase space appears to be regular, i.e., periodic and quasiperiodic motion. Exclusively bounded trajectories are encountered. The corresponding amplitude of the bounded energy variations during the driving cycles increases with increasing distance of the trajectories from the stable period one fixed point at the origin [see Figs. 2(a) and 2(b)]. Note that these statements hold significantly beyond the spatial scales shown in Fig. 3(a). This picture changes if we increase the amplitude to $\beta_1 = 0.5$; see Fig. 3(b). Now a regular island of the phase space centered around the fixed point at the origin is surrounded by an irregular point pattern. This pattern corresponds to the trajectories analyzed in Figs. 2(d)–2(f) showing a time evolution characterized by an average exponential increase in coordinate and energy space. Phase space can therefore be divided into two portions: one with bounded and one with unbounded motion. This picture persists with increasing frequency ω . For a given frequency and small driving amplitude β_1 low-energy phase space is regular. With increasing β_1 the phase space volume of the bounded regular motion decreases (see below), and gradually the phase space component consisting of “exponential motion” takes over.

For a large amplitude $\beta_1 = 1$ all of phase space consists of exponentially diverging trajectories, and no regular (or chaotic; see below) structures survive. Note that $\beta_1 = 1$ is the case where the lower turning point of the oscillating power of the TPO corresponds to power zero and is therefore subject to free, i.e., unconfined dynamics.

Beyond the above general statements, let us increase the frequency ω stepwise and see how the structures in the PSS change. Figure 3(c) shows the PSS for $\beta_1 = 0.5$ and $\omega = 0.3$. It exhibits a large centered regular island around the stable period one fixed at the origin. Decentered regular islands occur which correspond to period two stable fixed points at $(|q| = 33, |p| = 33.5)$. A hierarchical structure of smaller islands around these main ones can equally be observed. The sequence of PSS in Figs. 3(d)–3(f) is for an intermediate frequency $\omega = 1$ with increasing amplitude $\beta_1 = 0.15, 0.2, 0.9$ of the TPO. Figure 3(e) shows the PSS for $\omega = 1$ and $\beta_1 = 0.2$. It exhibits two large separated regular islands around period two fixed points which are off-center. The corresponding centered regular island (see the inset for its magnification) with the period one fixed point at the origin is of much smaller size. The two fixed points of the large decentered regular islands in Fig. 3(e) describe a two-mode left-right asymmetric motion in the oscillator potential accompanied by alternating phases of small- and large-amplitude motion. Off those large regular islands [see Fig. 3(e)] there is an area with many significantly smaller regular islands interdispersed in a sea of irregular motion.

We mention that trajectories starting from this mixed portion of phase space, which finally become unbounded with an exponential increase of their coordinate and momenta (energy), can beforehand show a long period of stickiness to the neighborhood of small regular islands in this regime. All outer parts of phase space [see Fig. 3(e) with a strongly depleted spread point pattern], as discussed above, correspond to exponentially diverging trajectories. Decreasing the amplitude β_1 leads to an increase of the size of the off-centered large islands. They will then take over a large part of the completely regular “low-energy” phase space of the TPO; see Fig. 3(d). In Fig. 3(d) regular islands around two period three fixed points also can be observed. Increasing the amplitude [see Fig. 3(f) for $\beta_1 = 0.9$ and $\omega = 1$] now shows a completely confined chaotic sea and only tiny regular structures within it. We note that for $\beta_1 > 0.5$ the above-discussed cusplike behavior [see corresponding discussion in the context of Fig. 1(a)] of the instantaneous potential of the TPO for $\beta < 0.5$ is the origin of an unstable behavior and resultingly chaotic sea in the immediate vicinity of the origin in the corresponding PSS. Again, outside this confined chaotic sea unbounded exponentially diverging trajectories take over.

Figure 3(g) addresses the case of a much larger frequency $\omega = 10$ for small-amplitude $\beta_1 = 0.1$. It shows again an exclusively regular phase space with one large centered main island with the period one fixed point. For the same frequency but $\beta_1 = 0.3$ Fig. 3(h) presents a two-component phase space again. The inner regular island around the period one fixed point shows subislands around a period four fixed point. The outer part of phase space corresponds exclusively to the exponentially diverging motion. We conclude that an amazingly broad frequency and amplitude regime is encountered within

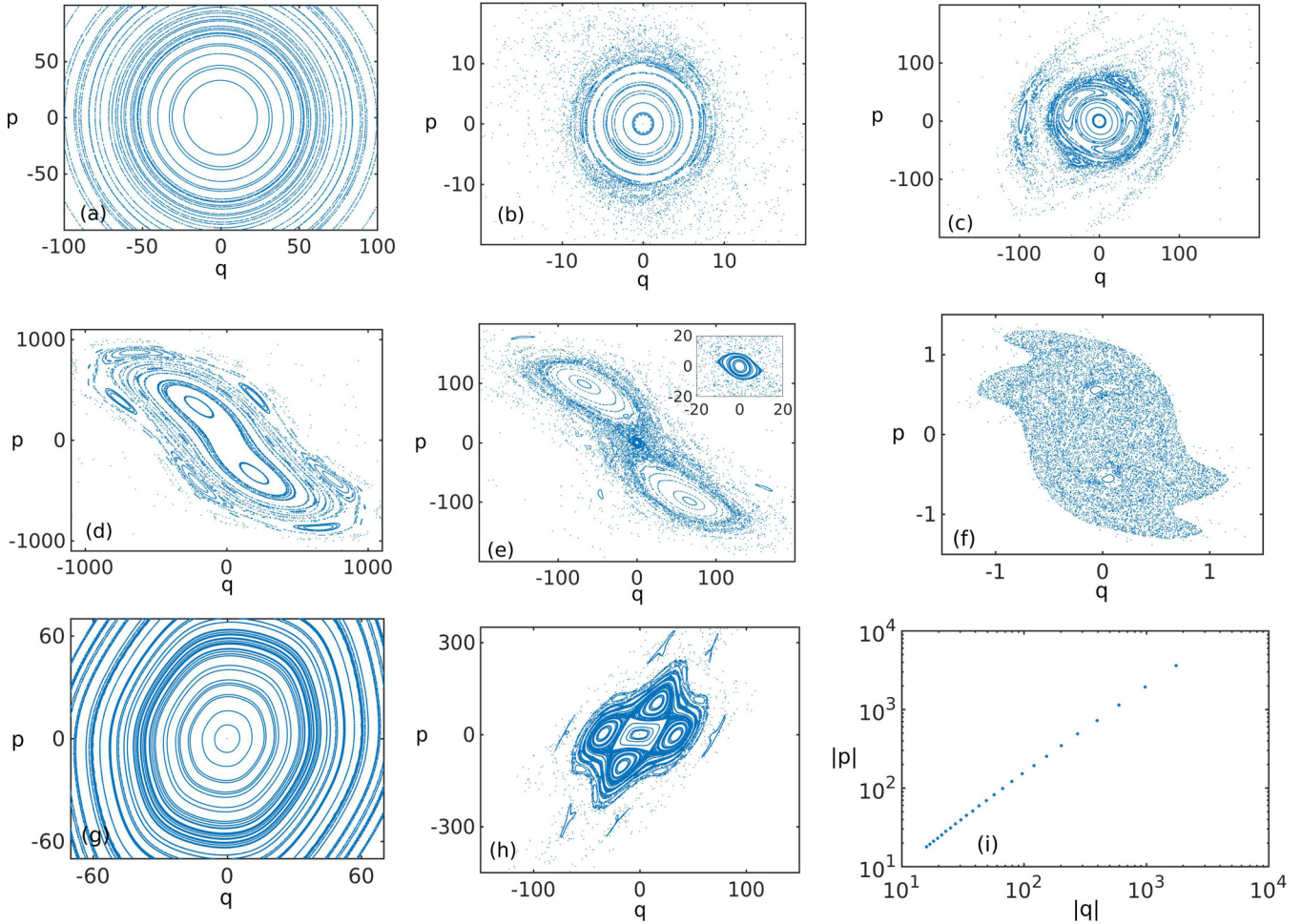


FIG. 3. Poincaré surfaces of section of phase space (q, p) . (a), (b) Low-frequency $\omega = 0.1$ and two different amplitudes $\beta_1 = 0.1$ and $\beta_1 = 0.5$, respectively. (c) A somewhat larger frequency and intermediate amplitude $\omega = 0.3$, $\beta_1 = 0.25$. (d)–(f) The cases $\omega = 1$ for $\beta_1 = 0.15, 0.2, 0.9$, respectively. (g), (h) The case of a larger frequency $\omega = 10$ with increasing amplitude $\beta_1 = 0.1$ and $\beta_1 = 0.3$, respectively. (i) The magnitude of the coordinates and momenta of the positions of the dominant period two fixed points of the PSS with varying β_1 on a double logarithmic scale. From large to small values in phase space the positions of the fixed points are indicated by crosses for which β_1 varies from 0.10 ($|q| = 1754, |p| = 3593$) to 0.34 ($|q| = 16.0, |p| = 17.8$) in steps of 0.01 for $\omega = 1$. Note the different scales of the subfigures.

which the underlying motion of the TPO is of composite character showing both a regular or mixed regular-chaotic bounded motion and an exponential unbounded dynamics. Finally Fig. 3(i) shows the positions (crosses) of the dominant period two stable fixed points of the PSS (period $2T = \frac{4\pi}{\omega}$ for the TPO) in phase space with varying amplitude β_1 and for the frequency $\omega = 1$. For $\beta_1 = 0.10$ the stable fixed point occurs at large distances ($|q| = 1754, |p| = 3593$) and provides the center of an equally large regular island. With increasing β_1 it moves inwards, i.e., towards the origin [shown in Fig. 3(i) in steps of 0.01 for β_1] and is accompanied by a shrinking of the size of the corresponding regular islands [see also Figs. 3(d) and 3(e) for $\omega = 1$ and $\beta_1 = 0.15, 0.2$ respectively]. Finally at approximately $\beta_1 = 0.34$ ($|q| = 16.0, |p| = 17.8$) this regular island and the stable fixed point disappear.

C. Quantification of phase space volumes and mean energy gain

Let us quantify the above observations. To this end we derive computational estimates of the volume V_{ps} of the phase space

that leads to bounded motion. The latter can be purely regular or of mixed regular-chaotic origin and changes with varying parameters such as the frequency ω and the amplitude β_1 . Knowing $V_{ps}(\omega, \beta_1)$ tells us how generic the exponentially diverging dynamics is which occupies the complementary part of phase space. $V_{ps}(\omega, \beta_1)$ therefore corresponds to the finite and bounded low-energy portion of phase space that “survives and resists” to the driving in the sense that the energy fluctuations in the course of the dynamics remain bounded. The unbounded complementary part of phase space is exclusively occupied by the exponentially diverging motion and infinite energy growth.

Figure 4 shows on a logarithmic scale the volume V_{ps} of phase space in the stroboscopic PSS with varying oscillation amplitude β_1 of the TPO. Three cases of different frequencies $\omega = 0.1, 1, 10$ are presented addressing comparatively low, intermediate, and higher frequencies. V_{ps} has been determined numerically by coarse graining the phase space in the PSS and approximately measuring the area of the corresponding (regular and chaotic) islands. Since V_{ps} varies over many

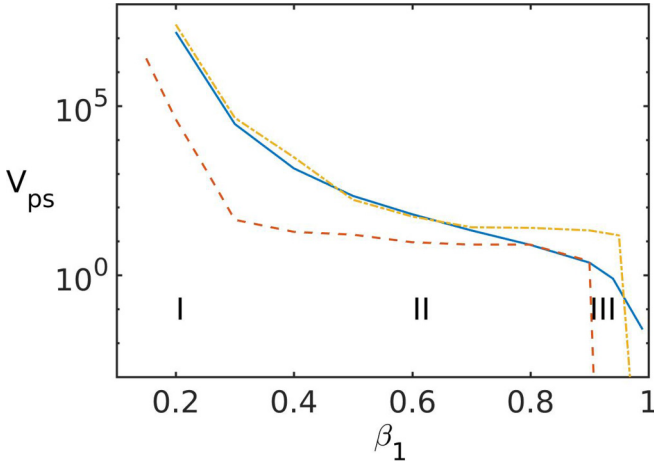


FIG. 4. Volume V_{ps} of phase space in the PSS which corresponds to the bounded motion with varying oscillation amplitude β_1 of the TPO. Full, dashed, and dash-dotted curves correspond to the frequencies $\omega = 0.1, 1, 10$, respectively. Note the logarithmic scale for V_{ps} .

orders of magnitude (see Fig. 4) with varying value of β_1 we are predominantly interested in a crude estimate of its value. Three different regimes I, II, and III can be distinguished in Fig. 4. For small amplitudes $\beta_1 \lesssim 0.25$ (regime I) the volume V_{ps} is extremely sensitive to the value of the amplitude β_1 of the TPO. It covers many orders of magnitude, e.g., decreasing from 2.5×10^6 to approximately 40 when β_1 increases only from 0.15 to 0.3 for the case of $\omega = 10$. This clearly demonstrates that for small amplitudes β_1 the phase space is rapidly taken over by regular and bounded motion in agreement with the above-discussed PSS [see Figs. 3(a), 3(d), and 3(g)]. The dependence of V_{ps} on β_1 becomes much weaker in the intermediate regime $0.3 \lesssim \beta_1 \lesssim 0.9$ (regime II), where, e.g., for the case $\omega = 1$ almost a plateau-like structure can be observed. While the volume V_{ps} of bounded motion does not change as much as in regime II as it does in regime I, the character of the confined motion could severely change. This is demonstrated in Figs. 3(f) and 3(h). For the low-frequency $\omega = 0.1$ a purely regular island of bounded motion occurs, whereas for an intermediate-frequency $\omega = 1$ a bounded chaotic sea is encountered. Finally, in regime III for $1 \geq \beta_1 \gtrsim 0.9$ we observe again a rapid decrease of V_{ps} for β_1 increasing from 0.9 to 1. In the limit $\beta_1 = 1$ we arrive at $V_{ps} = 0$, and all of phase space consists of exponentially diverging trajectories. Note that the corresponding transition needs to be by no way smooth. Its details depend on the destruction of the last invariant spanning manifolds, which could, as is, for example, the case for $\omega = 1$ and $\beta_1 > 0.9$ [see the confined chaotic sea in Fig. 3(f)], lead to a sudden transition from a finite bounded volume to zero volume.

It is instructive to consider not only individual trajectories in the regime of exponential growth but also the behavior of the mean of the energy \bar{E} and the corresponding standard deviation ΔE for an ensemble of trajectories with randomly chosen initial conditions in this regime. We note that these trajectories are sensitive to the initial conditions as it holds for any chaotic trajectory. Figure 5 shows these two quantities $\bar{E}, \Delta E$ as a

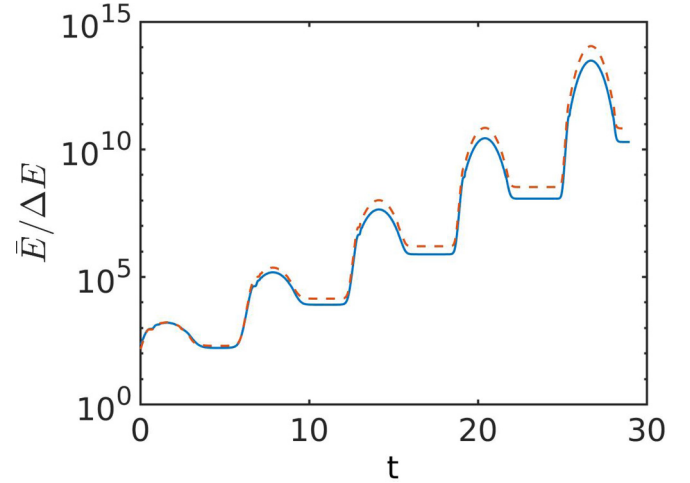


FIG. 5. Mean energy \bar{E} (full line) and its standard deviation ΔE (dashed line) as a function of time for a statistical ensemble of trajectories sampled from the exponentially accelerating part of the phase space for $\omega = 1$ and $\beta_1 = 0.9$.

function of time for 100 trajectories of the phase space for $\omega = 1, \beta_1 = 0.9$ [see also Fig. 3(f)]. The envelope behavior shows an exponential increase of both $\bar{E}, \Delta E$ where the standard deviation is slightly larger than the mean. The cycles of the “pumping” of the TPO (the period of the oscillator is here 2π) are clearly visible. Note the extraordinary large energy gain per cycle which amounts to two orders of magnitude in the energy per cycle. As such this oscillator is therefore an extremely efficient “accelerator” or energy pumping “device.” We remark that our numerical simulations have been performed for larger times than the ones shown in Fig. 5 and support this picture. However, with increasing propagation time the computational time to integrate one further oscillator period grows substantially and therefore limits the time evolution to be probed.

As already indicated in Sec. III A in the context of the discussion of individual trajectories we observe a rapid energy change for the first half-cycle $nT < t < (n + 1/2)T$ (n is a positive integer) for which the strong confinement of the TPO obeys $\beta(t) > \beta_0$. For a substantial part of the second half-cycle $(n + 1/2)T < t < (n + 1)T$ with the weaker confinement $\beta(t) < \beta_0$ the energy remains approximately unchanged (on the logarithmic scale of Fig. 5). This picture provides, however, an incomplete description of the growth of the energy. Indeed, the dynamics and time evolution of the energy is asymmetric with respect to the turning points of the TPO $(n + 1/4)T, (n + 3/4)T$ for both the first and second half-cycle. This asymmetry is particularly pronounced for the second half-cycle. Specifically, during the first quarter cycle $nT < t < (n + 1/4)T$ the energy increases, whereas it decreases to a slightly lesser extent during the second quarter-cycle $(n + 1/4)T < t < (n + 1/2)T$. At the beginning of the second half-cycle the energy saturates and remains approximately constant, but does so not for all of the second half-cycle. Instead it raises substantially again towards the end of the second half cycle, i.e., within the last quarter-cycle. This strong asymmetry leads to the net energy gain of the TPO.

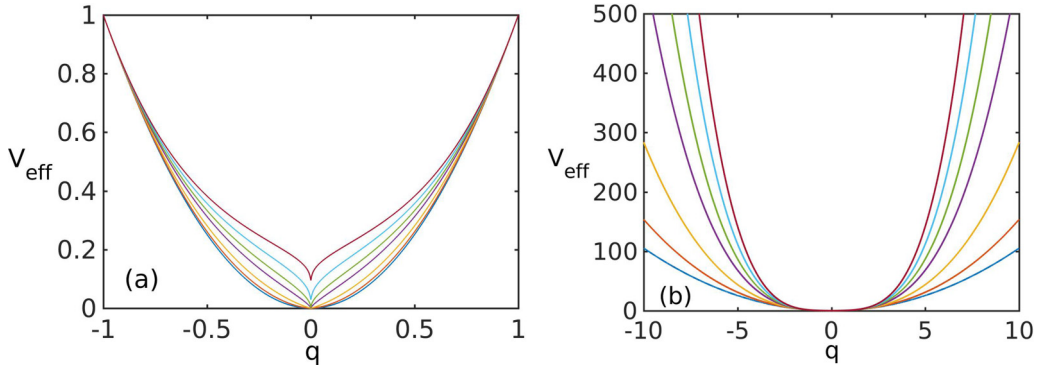


FIG. 6. Effective potential \mathcal{V}_{eff} in the high-frequency limit (see text) (a) in the vicinity of the origin and (b) for a larger q interval. The assignment of the values $\beta_1 = 0.1, 0.3, 0.5, 0.7, 0.8, 0.9, 0.99$ corresponds to the curves from bottom to top.

D. High-frequency regime

Finally let us discuss the dynamics of our TPO in the high-frequency limit $\omega \rightarrow \infty$. Obviously in this limit the largest frequency in the system is the one associated with the time-changing power of the TPO. A way to describe this situation is to average the rapidly oscillating potential over a period of the oscillation thereby obtaining an effective time-independent potential [19–24]

$$\mathcal{V}_{\text{eff}} = \frac{1}{T} \int_0^T \alpha q^{2\beta(t)} dt, \quad (2)$$

where we remind the reader that $\beta(t) = \beta_0 + \beta_1 \sin(\omega t)$. Due to the integration in Eq. (2) \mathcal{V}_{eff} is independent of the frequency ω and depends solely on β_0, β_1 . The question is how this autonomous (energy-conserving) one-dimensional potential, which leads to exclusively integrable, i.e., periodic motion, looks like. Or, in other words, which features of the different instantaneous power-law potentials reflect themselves in the time-averaged high-frequency limit leading to \mathcal{V}_{eff} . For potentials of a product form concerning their time and spatial dependence such as the parametrically driven harmonic oscillator $V_{po}(t) = \beta(t)q^2$ the shape of the time-averaged potential is the same as the original one. This is certainly not the case for our TPO. Rescaling time under the integral and accounting for the regularization of the power-law potential Eq. (2) becomes

$$\mathcal{V}_{\text{eff}} = \frac{\alpha}{2\pi} (q^2 + C)^{\beta_0} \int_0^{2\pi} (q^2 + C)^{\beta_1 \sin(t)} dt. \quad (3)$$

Exploiting the fact that the subintegrals in the intervals $[0, \frac{\pi}{2}]$ and $[\pi, \frac{3\pi}{2}]$ equal those in the intervals $[\frac{\pi}{2}, \pi]$ and $[\frac{3\pi}{2}, 2\pi]$, respectively, as well as employing the substitution $u = \beta_1 \sin(t)$ results in the following representation of the effective potential:

$$\begin{aligned} \mathcal{V}_{\text{eff}} &= \frac{\alpha}{\pi\beta_1} (q^2 + C)^{\beta_0} \int_0^{\beta_1} [(q^2 + C)^u - (q^2 + C)^{-u}] \\ &\quad \times \frac{1}{\sqrt{1 - (\frac{u}{\beta_1})^2}} du. \end{aligned} \quad (4)$$

The peculiarity of both representations of \mathcal{V}_{eff} in Eqs. (3) and (4) is the fact that the integration is performed with respect to the exponent of the integrand. As a result the integral cannot be expressed in terms of simple known analytical functions, i.e., it

has to be performed numerically. This goes hand in hand with our previous remark that in general any analytical approach to the TPO seems to be very difficult due to its time-dependent, in general fractional, exponent.

Figures 6(a) and 6(b) show the effective potential \mathcal{V}_{eff} in the high-frequency limit, as obtained by a numerical integration. Let us first focus on the behavior close to the origin, which is shown in Fig. 6(a). With increasing β_1 ranging from 0.1 to 0.7 the flat bottom of the potential around the origin develops into a linear rise. Further increasing the distance from the origin this linear behavior turns into a quadratic and subsequently higher order one. This happens because the linear scaling dominates in the integral for the effective potential \mathcal{V}_{eff} for very short distances as compared to the quadratic one. It is, however, “accessible” only within the TPO if the amplitude β_1 is sufficiently large. For $\beta_1 > 0.7$ the behavior close to the origin is characterized by a cusplike dip, which can be assigned to the dominance of the powers of the TPO being sublinear [see also the corresponding snapshots of the static potential of the TPO in Fig. 1(a)] and possesses for $C = 0$ diverging derivatives at the origin. For larger distances from the origin the potential changes its second derivative from negative to positive. All potentials become degenerate at $q = \pm 1$ independently of the value of β_1 . Figure 6(b) shows \mathcal{V}_{eff} on a larger spatial scale where a clear ordering with respect to the strength of the asymptotic ($q \rightarrow \infty$) confinement is visible. Larger amplitudes β_1 correspond to a stronger asymptotic confinement in this high-frequency limit. Finally let us compare the TPO dynamics and the dynamics in the time-independent effective potential \mathcal{V}_{eff} [see Eqs. (3) and (4)]. Figure 7 shows typical trajectories for the initial condition $[q(t=0) = 5, p(t=0) = 5]$ for both cases, where $\omega = 1000$ has been chosen for the TPO. The differences w.r.t. their dynamics not being visible for the finite resolution of Fig. 7 amount to maximally 0.1% for the propagation time shown. This confirms the validity of the high-frequency picture derived above. Let us shed some light on the behavior of the TPO with increasing frequency towards the high-frequency limit. The period T of the oscillations for our specific trajectory is $T = 3.7878$ for $\omega = 10$ and becomes $T = 3.7590$ for $\omega = 1000$, whereas the effective potential provides the value $T = 3.7588$. We note that the corresponding time-independent harmonic oscillator ($\alpha = 1, \beta_0 = 1, \beta_1 = 0$) amounts to $T = 4.4429$. These comparatively small deviations in the frequency should,

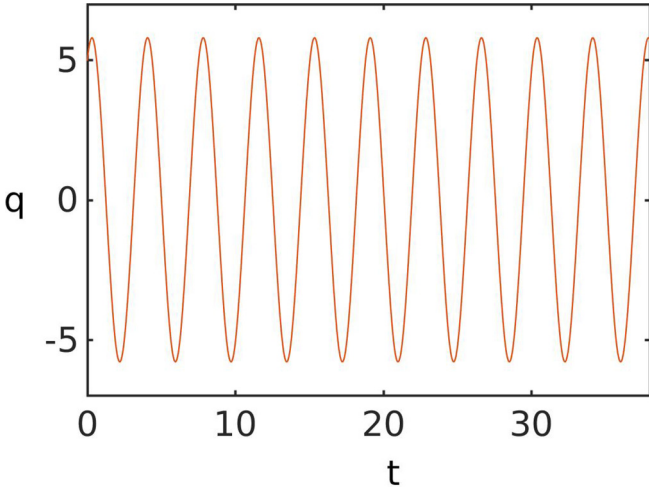


FIG. 7. Trajectories $q(t)$ in coordinate space with initial condition $q(t=0) = 5$, $p(t=0) = 5$ for both the TPO and the time-independent effective potential [see Eqs. (3) and (4)]. The two curves are indistinguishable, i.e., on top of each other on the resolution of the figure. The TPO parameters chosen are $\omega = 1000$, $\beta_1 = 0.3$.

however, not obscure the fact that there are major deviations between the cases $\omega = 10$ for the TPO and the effective potential dynamics for the trajectory $q(t)$, which amount up to 12%.

IV. CONCLUSIONS AND OUTLOOK

We have explored the nonlinear dynamics of the driven power-law oscillator with a focus on the analysis of the phase space structures and the possibility of energy gain of the oscillator. When comparing to the existing models for oscillators in the literature, the TPO appears to be of unusual appearance. Opposite to the kicked or parametrically driven oscillators which keep their shape during driving, the TPO continuously changes its shape in the course of a period of the periodic driving. Choosing as an equilibrium the harmonic oscillator, during one half-period of the driving the confinement strength of the anharmonic TPO is larger and during the other half-period the power of the confining potential is smaller when compared to the harmonic oscillator. With increasing amplitude of the oscillating power the oscillator potential can become linear or even inverse its curvature, such that the confining properties become correspondingly weak. In the latter case a cusp appears in the instantaneous potential that leads to kicks in the dynamics particularly relevant for low-velocity trajectories near the origin.

Our computational study has shown that for sufficiently large amplitude the TPO exhibits exponential acceleration and energy gain within the regime of phase space and timescales considered here. We conjecture that this holds even for an infinitely large part of the unbounded phase space. The structure of the finite low-energy part of the phase space around the origin exhibits bounded motion which can be completely regular (small-amplitude, arbitrary frequency) or mixed regular-chaotic (intermediate-amplitude) up to the case of a dominantly chaotic phase space (intermediate-amplitude

and frequency). We unraveled an intriguing mechanism of energy gain on the level of individual trajectories which links to the power-law pumping during the cycling of the TPO. Performing a corresponding statistical analysis we could assign the different periods of energy flow in and out of the oscillator to the phases of the external driving with the net result of an exponential energy gain. The exponential acceleration takes place in an amazingly broad parameter regime w.r.t. the frequency and amplitude of the TPO. The volume of phase space which corresponds to the bounded motion is extremely sensitive to the amplitude of the driving varying over many orders of magnitude and showing a rich structure. We remark that the observed exponential acceleration could potentially also be related to heating, which has very recently been found to occur in periodically driven many-particle systems [25] showing different “temperatures” after thermalization for slow and fast driving. Finally, in the high-frequency limit, an effective time-averaged and static potential has been determined which combines interesting features, such as the near origin cusp (for sufficiently large driving amplitude) and a very strong effective confinement at large distances. The exact dynamics reflects this high-frequency behavior only for large values of the frequency.

Although our driven power-law oscillator is a kind of oscillator with peculiar properties and as such, to our opinion, of interest on its own, let us briefly address possible experimental realizations. Of course, no experimental setup will ever lead to an infinitely spatially extended confinement such that any concrete realization will always probe the TPOs dynamics on finite timescales. This holds in particular w.r.t. the component of the exponentially diverging motion. Since the trapping technology of cold ions and especially of neutral atoms has advanced enormously during the past decades [26–29] there exists a huge flexibility concerning the design and the time-dependent change also of the shape of these traps. One can therefore use a gas of, e.g., thermal atoms for which interaction effects are negligible and “pump” the oscillator according to the TPO in order to finally perform absorption spectroscopy at different time instants and as a result observe the expansion dynamics of the atomic cloud. This is a microscopic example and in particular does not exclude the possibility of probing the TPO at hand of a macroscopic, i.e., mechanical setup. As can be seen from the time evolution of the energy of the oscillator our TPO is an extremely efficient “accelerator,” and one could in principle imagine its application as a few-cycle trap accelerator efficiently switching between different energy regimes.

As a look into the future, it might be interesting but very challenging to provide an analytical approach to the TPO in some of the accessible parameter regimes. However, it is not clear whether these plans are destined to fail, since even the simplest integrals cannot be expressed in terms of standard functions because it is typically the time-dependent exponent which is to be integrated. Still, a further more detailed analysis and understanding of the rich structure of the TPO is certainly desirable and, if not analytically, then computationally an interesting endeavor. Going one step further and analyzing the quantum TPO via, e.g., Floquet theory and identifying the characteristics of its Floquet spectrum is an intriguing perspective.

ACKNOWLEDGMENTS

This work has been in part performed during a visit to the Institute for Theoretical Atomic, Molecular and Optical

Physics (ITAMP) at the Harvard Smithsonian Center for Astrophysics in Cambridge, Massachusetts, whose hospitality is gratefully acknowledged. The author thanks B. Liebchen for a careful reading of the manuscript and valuable comments.

-
- [1] R. Weinstock, *Am. J. Phys.* **29**, 830 (1961); R. T. Bush, *ibid.* **41**, 738 (1973); A. Thorndike, *ibid.* **68**, 155 (2000); C. F. Farina and M. M. Gandelman, *ibid.* **58**, 491 (1990); K. R. Symon, *Mechanics*, 3rd ed. (Addison-Wesley Reading, MA, 1972); G. Flores-Hidalgo and F. A. Barone, *Eur. J. Phys.* **32**, 377 (2011).
- [2] I. Kovacic and M. J. Brennan (eds.), *The Duffing Equation, Nonlinear Oscillators and Their Behaviour* (Wiley, Chichester, UK, 2011).
- [3] H. J. Korsch, H. J. Jodl, and T. Hartmann, *Chaos* (Springer, Heidelberg, 2008).
- [4] L. E. Reichl, *The Transition to Chaos*, 2nd ed. (Springer, New York, 2004).
- [5] H. J. Stöckmann, *Quantum Chaos: An Introduction* (Cambridge University Press, Cambridge, UK, 1999).
- [6] T. I. Fossen and H. Nijmeijer, *Parametric Resonance in Dynamical Systems* (Springer, New York, 2011).
- [7] E. Fermi, *Phys. Rev.* **75**, 1169 (1949).
- [8] V. Gelfreich and D. Turaev, *J. Phys. A* **41**, 212003 (2008).
- [9] K. Shah, D. Turaev, and V. Rom-Kedar, *Phys. Rev. E* **81**, 056205 (2010).
- [10] B. Liebchen, R. Buechner, C. Petri, F. K. Diakonov, F. Lenz, and P. Schmelcher, *New J. Phys.* **13**, 093039 (2011).
- [11] K. Shah, *Phys. Rev. E* **88**, 024902 (2013).
- [12] V. Gelfreich, V. Rom-Kedar, K. Shah, and D. Turaev, *Phys. Rev. Lett.* **106**, 074101 (2011).
- [13] V. Gelfreich, V. Rom-Kedar, and D. Turaev, *Chaos* **22**, 033116 (2012).
- [14] B. Batistic, *Phys. Rev. E* **90**, 032909 (2014).
- [15] T. Pereira and D. Turaev, *Phys. Rev. E* **91**, 010901(R) (2015).
- [16] S. M. Ulam, in *Proceedings of the 4th Berkeley Symposium on Mathematical Statistics and Probability*, edited by J. Neyman (University of California Press, Berkeley, 1961), Vol. 3, pp. 315–320.
- [17] M. A. Lieberman and A. J. Lichtenberg, *Phys. Rev. A* **5**, 1852 (1972).
- [18] M. Robnik and V. G. Romanovski, *J. Phys. A* **39**, L35 (2006); D. Boccaletti and G. Pucacco, *Theory of Orbits 1 and 2* (Springer, Berlin, Heidelberg, New York, 2004).
- [19] I. Vorobeichik, R. Lefebvre, and N. Moiseyev, *Europhys. Lett.* **41**, 111 (1998).
- [20] P. K. Papachristou, E. Katifori, F. K. Diakonov, V. Constantoudis, and E. Mavrommatis, *Phys. Rev. E* **86**, 036213 (2012).
- [21] M. Gärtner, F. Lenz, C. Petri, F. K. Diakonov, and P. Schmelcher, *Phys. Rev. E* **81**, 051136 (2010).
- [22] F. R. N. Koch, F. Lenz, C. Petri, F. K. Diakonov, and P. Schmelcher, *Phys. Rev. E* **78**, 056204 (2008).
- [23] S. Rahav, I. Gilary, and S. Fishman, *Phys. Rev. Lett.* **91**, 110404 (2003).
- [24] S. Rahav, I. Gilary, and S. Fishman, *Phys. Rev. A* **68**, 013820 (2003).
- [25] M. Bukov, M. Heyl, D. A. Huse, and A. Polkovnikov, *Phys. Rev. B* **93**, 155132 (2016).
- [26] C. Schneider, M. Enderlein, T. Huber, and T. Schaetz, *Nat. Phot.* **4**, 772 (2010).
- [27] M. D. Hughes, B. Lekitsch, J. A. Broersma, and W. K. Hensinger, *Contemp. Phys.* **52**, 505 (2011).
- [28] G. Wilpers, P. See, P. Gill, and A. G. Sinclair, *Nat. Nanotech.* **7**, 572 (2012).
- [29] C. J. Pethick and H. Smith, *Bose-Einstein Condensation in Dilute Gases* (Cambridge University Press, Cambridge, UK, 2008).